

Single-atom resolved collective spectroscopy of a one-dimensional atomic array

Britton Hofer,^{*} Damien Bloch,^{*} Giulio Biagioni, Nathan Bonvalet, Antoine Browaeys, and Igor Ferrier-Barbut[†]
*Université Paris-Saclay, Institut d'Optique Graduate School,
CNRS, Laboratoire Charles Fabry, 91127, Palaiseau, France*

Ordered atomic arrays feature an enhanced collective optical response compared to random atomic ensembles due to constructive interference in resonant dipole-dipole interactions. One consequence is the existence of a large shift of the transition with respect to the bare atomic frequency. In the linear optics regime (low light intensity), one observes a spectroscopic shift of the Lorentzian atomic line often called the collective Lamb shift. For stronger driving, many excitations are present in the system rendering the calculation of this shift theoretically challenging, but its understanding is important for instance when performing Ramsey spectroscopy in optical clocks. Here we report on the study of the collective optical response of a one-dimensional array of 30 dysprosium atoms. We drive the atoms on the narrow intercombination transition isolating a 2-level system, and measure the atomic state with single-shot state readout using a broad transition. In the linear optics regime, we measure the shift of the resonance in steady state due to dipole interactions, and measure how this shift depends on the interatomic distance. We further resolve at the single atom level how the excitation is distributed over the array. Then, on the same transition we perform Ramsey spectroscopy *i. e.* away from the linear regime. We observe a time-dependent shift, that allows us to draw the connection between the collective Lamb shift observed in the linear optics regime and in the large-excitation case.

I. INTRODUCTION

Collective light-matter interactions in atomic ensembles is an example of a dissipative quantum many-body problem that has been studied for decades, both theoretically and experimentally [1–3]. Recent progress in atomic physics has led to new investigations in different directions. Particular experimental attention has been devoted to the understanding of the shift of an atomic transition due to resonant dipole-dipole interactions, the so-called collective Lamb shift [4]. On the one hand, many works have probed the shift of a Lorentzian line [5–12], in the regime of *low* light intensity where the atomic dipoles behave linearly and can be considered as classical. On the other hand, it is important to understand this shift in the context of optical clocks [13–16], where one typically performs Ramsey spectroscopy, *i. e.* outside the linear regime, where the non-linear response of single atoms cannot be ignored. In addition, in such systems, the atoms are usually ordered. The influence of geometrical order on the collective response of an atomic ensemble to light is now the topic of an intense research activity [10, 17–21], and the enhanced collective response of two-dimensional arrays in the linear optics regime has been investigated experimentally [22, 23].

In this context, we present here an experiment that probes the collective shift in a tweezer-based one-dimensional array of two-level atoms, both performing fluorescence spectroscopy in the classical (linear optics) regime *and* Ramsey spectroscopy in the quantum (non-linear) regime. Thanks to single-atom state readout using a combination of narrow and broad optical transitions [24], we reveal the microscopic effect

of collective resonant dipole-dipole interactions *at the single atom level*, and show experimentally how the clock shift in Ramsey spectroscopy is related to the line shift in the linear regime.

II. EXPERIMENTAL SETUP

To probe the collective Lamb shift in an ordered one-dimensional system, we prepare arrays of single dysprosium (Dy) atoms using the experimental platform presented in [25, 26]. The atoms are held in optical tweezers with a wavelength of 532nm. We produce ordered arrays of 30 atoms, with a controllable inter-tweezer spacing d from 1.25 μm to $\approx 4.5\mu\text{m}$. These arrays are obtained by rearranging a randomly loaded chain of 75 tweezers [27].

In the tweezers, the radial trap frequency is $\omega_r/(2\pi) = 50\text{kHz}$ while the axial one is $\omega_z/(2\pi) = 7\text{kHz}$. Given the atomic temperature in the tweezers $T = 5.5\mu\text{K}$, this yields a radial positional disorder of size $\sigma_r \simeq 50\text{nm}$ and an axial one of $\sigma_z \simeq 400\text{nm}$. This axial disorder is non-negligible with respect to the interatomic distance and hinders collective effects. In order to reduce disorder, we add an extra confinement along the tweezers' axis using an optical lattice produced by two 532nm beams interfering at a half angle of about 5° , yielding a lattice spacing of 3 μm (see Fig. 1). All atoms are loaded in a single lattice plane [28], perpendicular to the tweezers' axis. We give details in appendix A. Adiabatically turning this lattice on increases the axial trapping frequency up to $\omega_z/(2\pi) = 35\text{kHz}$ at the cost of an increased temperature of $T = 8.5\mu\text{K}$, resulting in final sizes $\sigma_r \simeq 70\text{nm}$ and $\sigma_z \simeq 90\text{nm}$ in these near-spherical traps.

Having prepared this 1D ordered system, we perform spectroscopy on the intercombination transition of ^{162}Dy with wavelength $\lambda = 626\text{nm} = 2\pi/k$

^{*} These authors contributed equally

[†] igor.ferrier-barbut@institutoptique.fr

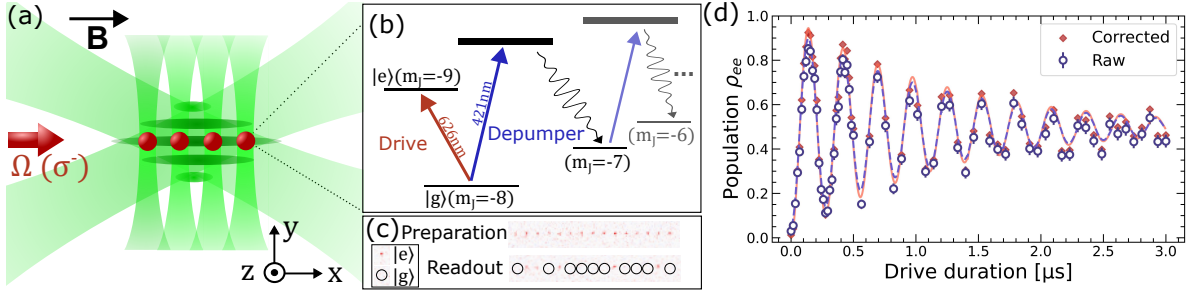


FIG. 1. (a) Schematic of the experiment: We perform spectroscopy on an array of Dy atoms held in optical tweezers of wavelength 532 nm and further confined along the weak trapping axis of the tweezers with a shallow-angle optical lattice, also at 532 nm. The red arrow shows the propagation direction of the driving laser with which we excite the atoms. (b) Dysprosium’s optical transitions used in this work. Spectroscopy is performed on the 626 nm intercombination line between $|g\rangle = |m_J = -8\rangle$ and $|e\rangle = |m_J = -9\rangle$ (linewidth $\Gamma = (2\pi) 135$ kHz). The broad 421 nm line ($\Gamma_{421} = (2\pi) 32.5$ MHz) is used to perform single-shot state readout by rapidly depumping atoms out of $|g\rangle$. (c) Readout of the atomic state in a single shot. The atom is reimaged if it was shelved in $|e\rangle$ and atoms in $|g\rangle$ were depumped to higher m_J states and are thus not re-imaged. (d) Measurement of the excited state fraction during Rabi oscillations for independent atoms, using the shelving technique illustrated in (b). The blue circles are raw data, while the red diamonds include corrections for detection errors (see appendix B). Error bars represent standard error on the mean. The lines represent solutions of the optical Bloch equations.

and linewidth $\Gamma = (2\pi) 135$ kHz which connects a $J = 8$ to a $J = 9$ Zeeman manifold [excited state $4f^{10}(^5I_8)6s6p(^3P^o_1)(8, 1)^o_9$] [29]. We isolate a two-level transition between $|g\rangle = |J = 8, m_J = -8\rangle$ and $|e\rangle = |J = 9, m_J = -9\rangle$ by applying a magnetic field of 7 G and tuning the driving laser to the σ^- transition frequency (the π transition is detuned by about 13 MHz). While the tweezers are magic for the $|g\rangle \rightarrow |e\rangle$ transition thanks to an elliptical polarization [25, 26], the lattice is linearly polarized perpendicular to the tweezer axis, and hence non-magic. As a consequence all experiments reported here are performed in free space (the tweezers and the lattice are turned off) to avoid inhomogeneous light shifts. The residual atomic motion during the free flight is negligible ($< 0.2\lambda$). In all the experiments we report, the light scattering sequence takes place on a time-scale shorter than $10\mu\text{s}$ such that we recapture the atoms with a high probability [25].

Nearly all studies of light scattering in free space rely on measurements of the radiated light. However, the theoretical description of this problem computes the many-body atomic density matrix, and the radiated field is calculated as a linear superposition of the atomic dipoles [30]. As such it is interesting to directly access the atomic state [24]. Here we use a method based on shelving [31, 32] from a broad transition [excited state $4f^{10}(^5I_8)6s6p(^1P^o_1)(8, 1)^o_9$, wavelength 421 nm, $\Gamma_{421} = (2\pi) 32.5$ MHz] to readout the internal state (see Fig. S2 and detailed in appendix B). Briefly, we apply an optical depumping pulse ($\tau_p = 100$ ns) on the broad transition with π polarization. This pulse depumps $|g\rangle$ atoms to other Zeeman states with $m_J > -8$. Atoms in $|e\rangle$ do not significantly decay in this interval as the lifetime of atoms in $|e\rangle$ is $\tau = 1/\Gamma = 1.2\mu\text{s}$. After the pulse, $|e\rangle$ atoms decay to $|g\rangle$. We re-image only the atoms

left in $|g\rangle$, while those in the other Zeeman states are not imaged. With this, we project the atomic state and image only the atoms that were in $|e\rangle$ before the blue depumping pulse. We thus obtain state readout (*i.e.* measurement of ρ_{ee}) of single atoms in a single shot with a fidelity limited by the excited state lifetime $F = 0.92 \simeq e^{-\tau_p/\tau}$. This method is in principle lossless if the atoms are efficiently repumped to $|g\rangle$ at the end of an experimental cycle. This would greatly improve the duty cycle, and we leave its implementation to future works. Fig. 1(c) shows an example of Rabi oscillations measured with this method.

III. LINEAR OPTICS REGIME

To benchmark the experiment, we first measure the collective frequency shift (δ_{spectro}) of the atomic line due to interactions [5, 10], Fig. 2. For this, we excite the atoms with a near-resonant laser, detuned by an amount Δ_L from the bare atomic resonance, with low intensity $I = 1.3 I_{\text{sat}}$ *i.e.* Rabi frequency $\Omega = (2\pi) 110$ kHz = 0.8Γ . This laser propagates either along the chain, or perpendicular to it. In the case where the drive runs parallel to the chain $\vec{k}_{\text{las}} = k\hat{x}$, the propagation phases of the fields radiated by each atomic dipole are the same as the propagation phase of the drive $e^{i\vec{k}_{\text{las}}\cdot\vec{r}} = e^{ikx}$. This results in an interference of the resonant dipole-dipole interactions [33], with a buildup of the interactions along the chain, resulting in a shift of the transition. In the perpendicular case this coherent buildup does not occur and only a weak shift is expected. Theoretically, the shift in steady state in the linear regime is given by the average interaction energy in the array [13]: $\delta_{\text{spectro}} = (1/2) \sum_{n \neq m} \text{Re}[V_{\text{dd}}(\vec{r}_n - \vec{r}_m)]$, where V_{dd} is the resonant dipole-dipole interaction ($\propto 1/d$

at large distances, see appendix D). Here, we perform time-dependent numerical simulations of the dynamics within a mean-field approximation [10]. They account for the finite time of the pulse and averaging over thermal positional disorder, (we typically find good agreement with the analytical formula). We present these predictions as solid lines in Fig. 2, showing good agreement with the data.

As stated above, the resonance shift in a 1D system is due to a buildup of the interaction along the chain. At the single atom level, this should result in an excitation probability that varies along the chain [33]. Thanks to single atom state readout, we can now directly measure how the excitation probability evolves along the chain. For a non-interacting system, it should be flat. We however observe a different behavior, visible in Fig. 3, where we plot the excitation probability of each individual atom in the chain. We present the data for two different detunings, taken over several days, with different Rabi frequencies (in the linear regime), such that the absolute excitation probability is meaningless. To compare it to theory we thus normalize the excitation probability to that of the first atom in the chain. Since this first point is prone to statistical noise, this normalization results in a statistical offset of all points, but we use it to keep the data analysis free of adjustable parameters (see more details in appendix C). For a positive detuning ($\Delta_L = +\Gamma/2$), we observe a *decay* of the excitation probability along the chain, in the direction

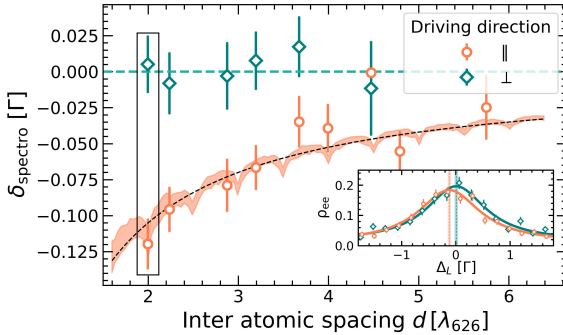


FIG. 2. Collective frequency shift of a 1D chain of 30 atoms: shift of the center of the resonance line when the atomic spacing is varied. The Rabi frequency of the drive is $\Omega = 0.80(8)\Gamma$. The orange circles correspond to a drive along the chain and the green diamonds to a perpendicular drive. Error bars represent standard error on the mean. When the driving laser is sent parallel to the chain, a frequency shift is observed that increases as the atoms get closer. In solid orange is the result of mean-field simulations accounting for positional disorder due to temperature. The shaded area accounts for the 10% uncertainty of the Rabi frequency of the drive. We also include a guide to the eye showing the $1/d$ dependence of the dipole-dipole interaction as seen with the black dashed line. The inset shows the measurement of the atomic line for the two points highlighted by the black box.

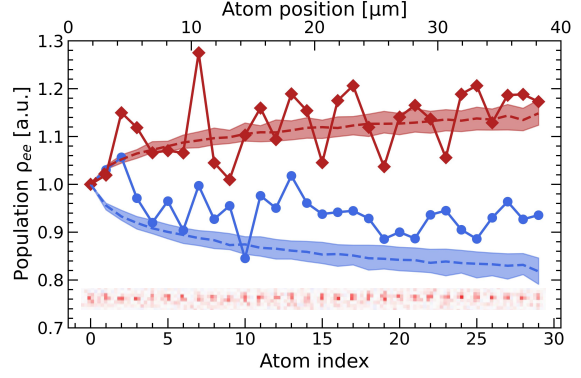


FIG. 3. Position-resolved excited state fraction. A driving beam detuned by $\Delta_L = \pm\Gamma/2$ is sent along the atomic chain from left to right. The atoms are $1.4\mu\text{m} = 2.2\lambda$ apart. The joined red (blue) diamonds (dots) are the experimental data for $\Delta_L = -\Gamma/2$ ($+\Gamma/2$), normalized to the fraction on the first atom. The dashed lines show mean-field simulation results averaged over thermal positional disorder. One observes a decay or growth of excitation along the chain depending on the detuning. The shaded area around the simulations accounts for a 10% uncertainty of the Rabi frequency.

of the drive's propagation. For a negative detuning ($\Delta_L = -\Gamma/2$), we observe an *increase* of the excitation along the chain. This behaviour was predicted in [33], and our experiment constitutes its observation *at the single atom level*. The dependence of the excitation probability on the position in the chain is due to the fact that the radiated atomic fields are either in phase ($\Delta_L < 0$) or out of phase ($\Delta_L > 0$) with the driving laser, and thus increase or decrease the effective driving strength and hence excitation probability. One might also explain the enhancement of the atomic excitation on the red side of the resonance as the first atoms focusing the field, increasing its value on the last atoms downstream, hence acting as an effective lens, seen here at the single atom level.

The results presented so far were obtained in the low light intensity regime where the atoms behave as classical dipoles [34]. Away from this limit, when many atoms are excited, one has to consider the full Hilbert space and non-trivial correlations should emerge at short interatomic distances [21, 35–37]. Ramsey spectroscopy is an example where one operates far from the classical regime. Here, we explore in this simple system of 30 atoms how the shift measured above in the classical regime and in steady state can be related to the shift observed in Ramsey spectroscopy.

IV. RAMSEY SPECTROSCOPY

To depart from the linear optics regime, we first measure the line shift in steady state as above, sim-

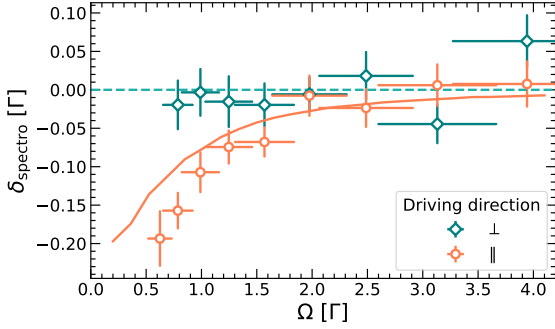


FIG. 4. Frequency shift of the maximum of the excitation fraction measured in steady state, as a function of driving power for a fixed inter-atomic distance of $d = 1.25\mu\text{m} = 2\lambda$. Error bars represent standard error on the mean. As the drive becomes too strong, the atomic dipole is progressively reduced causing the collective shift to vanish. The solid line is the result of mean-field simulations.

ply increasing the drive Rabi frequency to $\Omega > \Gamma$. We represent in Fig. 4 the position of the center of the line, as a function of the Rabi frequency of the drive. The experimental data is still taken in steady state after driving for $7\mu\text{s} \gg 1/\Gamma$. When increasing the Rabi frequency the line is broadened. In order to focus on the line shift, the data is acquired in a small 500kHz range. We also perform mean-field simulations at various Rabi frequencies. [38]. The results are represented as a solid line in Fig. 4, they reproduce the data well. We observe, in agreement with our previous work [10], that the shift is suppressed as soon as the Rabi frequency is on the order of Γ . As explained in [10], the shift suppression is due to the fact that the average atomic dipole ($\propto \rho_{eg}$) in steady-state vanishes like $\sim 1/\Omega$.

However, Ramsey spectroscopy does not operate in steady state. The atomic dipoles are initialized to a non-zero value by a first pulse with duration $\ll 1/\Gamma$ and area θ_0 . The dipoles then evolve without drive before the second pulse. The shift of the transition δ_{Ramsey} can be calculated in a mean-field approximation, assuming that the time between the two pulses is very short ($T_{\text{Ramsey}} \ll 1/\Gamma$): in this case one obtains $\delta_{\text{Ramsey}} = \delta_{\text{spectro}} \cos \theta_0$ [13]. The shift of the Ramsey fringes depends on the amount of excitation $\rho_{ee} = (1 - \cos \theta_0)/2$, as observed in [16]. This formula is valid only for $T_{\text{Ramsey}} \ll 1/\Gamma$. For longer times, the excitation decays due to spontaneous emission. As a consequence, one expects a *time-dependent* shift for Ramsey interferometry in the regime $T_{\text{Ramsey}} \sim 1/\Gamma$. The time dependence of the shift was theoretically investigated for short times and with a pulse area $\theta_0 = \pi/2$ in ref. [13] longer times and other pulse areas were considered in [15] (for a 3D ensemble). This time-dependence of the shift in Ramsey interferometry was never observed experimentally to the best of our knowledge.

To investigate it, we perform a Ramsey spec-

troscopy experiment on the $|g\rangle \rightarrow |e\rangle$ transition with a chain of 30 atoms. The short pulses (area θ_0) are

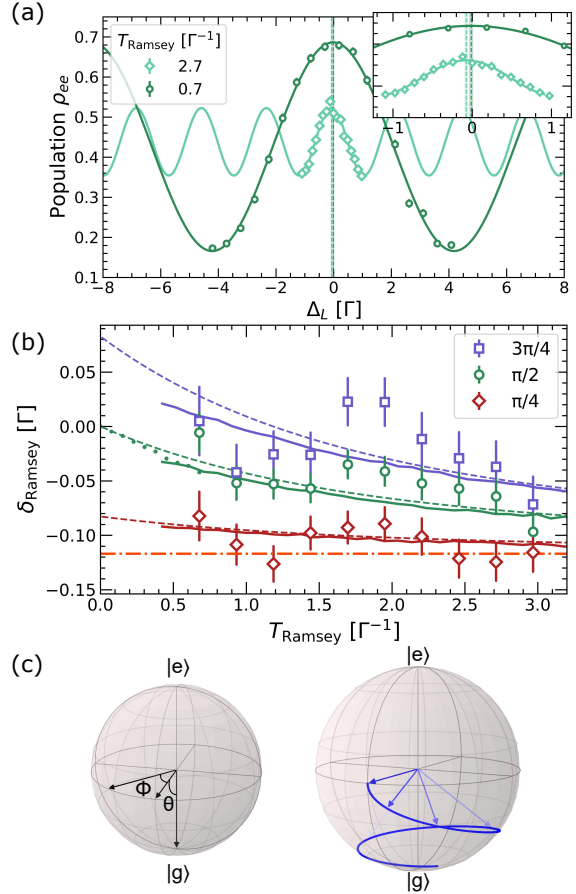


FIG. 5. (a) Ramsey fringes with a fixed pulse area $\theta_0 = \pi/2$ for two different T_{Ramsey} times corresponding to the free evolution time between the two pulses. (b) Time-dependent shift measured in Ramsey spectroscopy when changing the time T_{Ramsey} between the two pulses, for three different pulse areas θ_0 . For this experiment, the atoms are $1.4\mu\text{m} = 2.2\lambda$ apart and the drive's Rabi frequency is $\Omega = (2\pi)3\text{MHz} = 22\Gamma$. Error bars represent standard error on the mean. Results of the mean field simulations are shown as solid lines. The dashed-dotted horizontal orange line is the predicted δ_{spectro} shift calculated in the low-intensity regime with the mean field simulations. The data exhibits a time dependence in agreement with theory, connecting the large excitation regime of Ramsey spectroscopy to the low-excitation linear regime of fluorescence spectroscopy. The dotted green line shows the linear expansion for $\pi/2$ pulses from [13] in the limit where $T_{\text{Ramsey}}\Gamma \ll 1$. We use an ansatz with an excitation-dependent instantaneous shift (see main text), plotted with dashed lines for each θ_0 . (c) Schematic representation of the origin of the time-varying shift. Bloch sphere representation of the state of an atom during the time evolution T_{Ramsey} between the two Ramsey pulses. Following a $\pi/2$ pulse the Bloch vector precesses around the z axis at a varying rate: initially $\phi = 0$ while it reaches a non-zero value once the excitation has decayed, resulting in a shift which depends on the free evolution time.

created by a fiber electro-optic modulator with rise time ~ 1 ns, and an additional AOM for good extinction. For this dataset, the atoms were not trapped in the lattice before the release in free-space [39], which results in a lower shift of the transition. We perform a simple sequence of two pulses separated by a time T_{Ramsey} as considered in [13]. We pick three pulse areas: $\pi/4$, $\pi/2$ and $3\pi/4$. For each pulse area, we measure Ramsey fringes as a function of the laser detuning Δ_L (see Fig. 5(a)) and we record the position of the central fringe. We repeat the experiments for different T_{Ramsey} times between $0.8\mu\text{s} = 0.7\Gamma^{-1}$ and $3.5\mu\text{s} = 2.7\Gamma^{-1}$, see Fig. 5(b).

Our observations are reported in Fig. 5(b), well reproduced by mean-field solutions of the master equation (solid colored lines). They exhibit a dependence on the pulse area, as reported in [16]. However the striking feature is that the collective Lamb shift *evolves in time*, with a slope that depends on the pulse area. For the smallest one ($\pi/4$), we find a nearly time-independent shift with a value close to the expected spectroscopic shift (dashed-dotted orange line). For larger pulse areas the shift decays in time in agreement with the qualitative explanation given above, we discuss the implication of those findings below.

The data of Fig. 5(b) imply that the Bloch vector of an atom precesses at a varying frequency during the time separating the two pulses. To illustrate this, let us take the case of $\pi/2$ pulses, with the laser having a zero detuning with respect to the atomic resonance. In this case the precession rate starts from the initial value of $\dot{\phi}(t=0) = \delta_{\text{spectro}} \cos \theta_0 = 0$, leading to a zero shift for short wait times ($T_{\text{Ramsey}}\Gamma \ll 1$). As explained in ref. [13], this zero initial shift at $\theta_0 = \pi/2$ can be formally understood writing the contribution of other atoms to the time evolution of an atomic dipole: $(\dot{\rho}_{eg})_{\text{int}} = i\Omega_{\text{atoms}}(1 - 2\rho_{ee})/2$ where Ω_{atoms} is the Rabi frequency of the field radiated by the other atoms (see equation (S1)). For a $\pi/2$ pulse, $\rho_{ee} = 1/2$ and the dipole is not impacted by the others. Intuitively, this is due to the fact that during the free evolution time, the other atomic dipoles oscillate at the bare atomic frequency, and thus create an effective drive *in the equatorial plane* of the Bloch sphere. This field thus does not drive a precession in the equatorial plane ($\dot{\phi} = 0$) and does not lead to a shift of the transition for $\Gamma T_{\text{Ramsey}} \ll 1$.

For longer times ($T_{\text{Ramsey}}\Gamma \gtrsim 1$), the situation is different. As ρ_{ee} decays, the dipole evolution starts to depend on the other atoms. The authors of [13] derived a short-time linear expansion represented as a dotted line in Fig. 5(b). Here, we further use a simple ansatz to understand the time evolution of the shift. We assume that the instantaneous precession rate is given by $\dot{\phi} = \delta_{\text{spectro}} \cos \theta(t)$, and that $\cos \theta(t)$ is simply described by the single atom decay rate $\rho_{ee}(t) = \rho_{ee}(0)e^{-\Gamma t} = (1 - \cos \theta(t))/2$ [40]. This evolution is schematically represented on Fig. 5(c). Then the shift

of the Ramsey fringes for a time T_{Ramsey} is given by

$$\begin{aligned} \delta_{\text{Ramsey}} &= \frac{1}{T_{\text{Ramsey}}} \int_0^{T_{\text{Ramsey}}} \dot{\phi} dt \\ &= \delta_{\text{spectro}} \left[1 - (1 - e^{-\Gamma T_{\text{Ramsey}}}) \frac{1 - \cos \theta_0}{\Gamma T_{\text{Ramsey}}} \right]. \end{aligned}$$

The result is represented as dashed lines in Fig. 5(b), and reproduces the experimental data and mean-field simulations well. At long times ($\Gamma T_{\text{Ramsey}} > 1$ for which $\theta \rightarrow 0$), the precession rate approaches the value $\dot{\phi} = \delta_{\text{spectro}}$. Hence, the measured shift of Ramsey fringes converges towards δ_{spectro} . This allows to understand the observations of Fig. 5.

This data establishes a connection between the two regimes of the collective Lamb shift: in Ramsey spectroscopy the shift depends on the amount of excitation in the system, but as time evolves the shift converges to the low-excitation limit due to the decay of the excited state, and one recovers the shift measured in linear-optics fluorescence spectroscopy. The time dependence of the collective Lamb shift reported here matches the mean-field expectations. For shorter interatomic distances, one expects a departure from the mean-field predictions, opening the possibility to test beyond mean-field theories [15].

V. CONCLUSIONS

To conclude, we used a single atom tweezer platform to explore collective light scattering in atomic ensembles. On the one hand the single atom resolution brings an understanding to the microscopic origin of the observed collective effects. On the other hand, atomic state readout allows for the connection between different regimes of spectroscopy in the same platform. This opens new directions for studying light scattering in arrays, from the study of superradiance and atomic correlations induced by collective dissipation [36, 41] to the steady-state of driven-dissipative spin arrays [42–45].

ACKNOWLEDGMENTS

This project has received funding by the Agence Nationale de la Recherche (JCJC grant DEAR, ANR-22-PETQ-0004 France 2030, project QuBitAF), by the European Union (ERC StG CORSAIR, 101039361, ERC AdG ATARAXIA 101018511), and the Horizon Europe programme HORIZON-CL4-2022-QUANTUM-02- SGA (project 101113690 PASQuanS2.1).

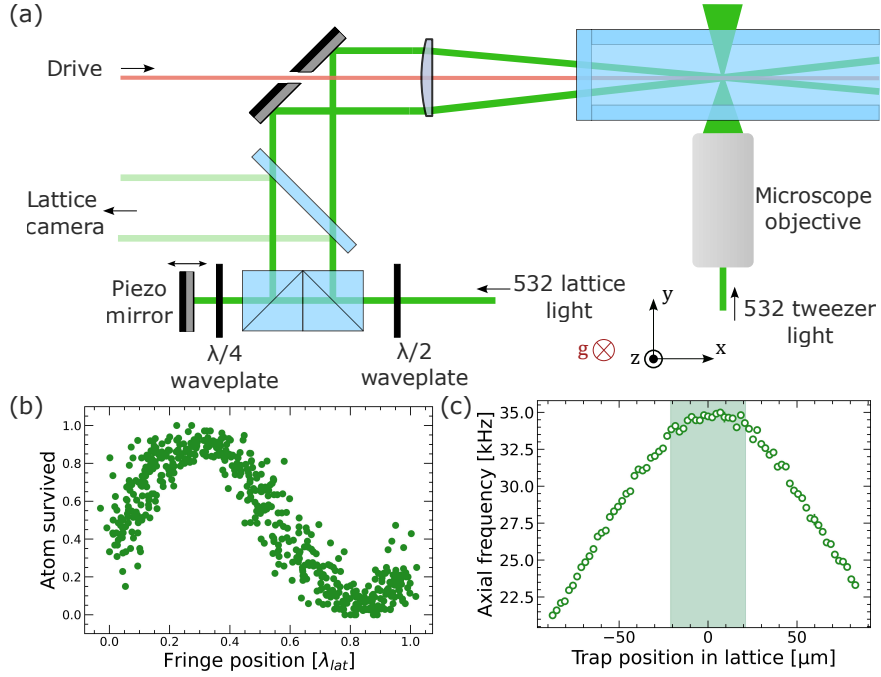


FIG. S1. (a) View from above of the optical setup for the light sheet creating additional axial confinement in the y direction. (b) Atom survival as we abruptly switch the lattice on for different positions of the bright fringe on the atoms. (c) Measurement of the axial trapping frequency across the chain. In order to have a homogeneous axial trapping frequency along the chain we only use the shaded area which corresponds to 30 atoms with a $1.4 \mu\text{m}$ spacing.

APPENDIX A: SHALLOW-ANGLE LATTICE

As presented in the main text, we impose an additional confinement along the tweezers' axial direction by using a shallow angle lattice. This lattice is made by interfering two beams of wavelength $\lambda_l = 532 \text{ nm}$ at the position of the tweezers (Fig. S1a). The lattice beams are off resonance from the tweezer beams by more than 300 MHz to avoid any unwanted interference. With this lattice, the axial confinement increases from 7 kHz up to 35 kHz on the central lattice sites where we perform the experiment. The lattice beams' waist is $10 \mu\text{m}$ at the atoms' position. The half-angle between the two beams is $\alpha = 5^\circ$ yielding a lattice spacing of $\lambda_l/2 \sin \alpha = 3 \mu\text{m}$. The lattice angle and beam waist (Rayleigh length $\approx 150 \mu\text{m}$) are chosen to obtain a relatively homogeneous axial trapping frequency across the chain of 30 atoms (see figure S1(c)). We load all of the atoms into only one bright fringe of the lattice because the planes are far apart due to the large lattice spacing. To generate the two beams we use two cubes and a mirror on a 3-axis-mount. The retroreflection mirror is mounted on a piezo stack to control the phase difference between the beams and place the central fringe on the atoms. The position of the lattice fringe is stabilized by monitoring the fringes on a camera. The lattice beams are sampled shortly before the atoms (see Fig. S1(a)). The relative phase between the beams on the camera and the beams on the atoms nevertheless drifts, result-

ing in a slow drift of the position of the bright fringe. To monitor this, we measure the fringe position directly on the atoms in the following way. At the end of every experimental sequence we abruptly turn the lattice on and off, the atoms only survive this lattice pulse when the bright fringe is on the atom since it exerts no center-of-mass kick (see Fig. S1(b)). By tracing the atoms' survival to this lattice pulse over time we can determine if the position of the bright fringe slowly drifts and we then correct for it.

APPENDIX B: SINGLE-SHOT STATE READOUT

In a typical experimental sequence, one atom scatters on the order of one to a few photons during the drive. Given a typical collection efficiency (a few %), it is impossible to measure the scattered photons in a single shot. Instead, we directly measure the internal state of each atom at a given time. This can be done because the transition that we use has a linewidth of $\Gamma_{626} = 2\pi \times 135 \text{ kHz}$ *i. e.* a lifetime of $|e\rangle$ of $1.2 \mu\text{s}$ which is relatively long. In particular it is much longer than the time it takes to scatter a few photons on the broad transition ($\Gamma_{421} = 2\pi \times 32 \text{ MHz}$). We apply a 100 ns pulse of 421 nm light. To generate this pulse, we use an AOM with a rise time around 100 ns followed by a Pockels cell EOM with a 10 ns rise time. The light has linear polarization along the magnetic field axis to excite the π transition. The atoms

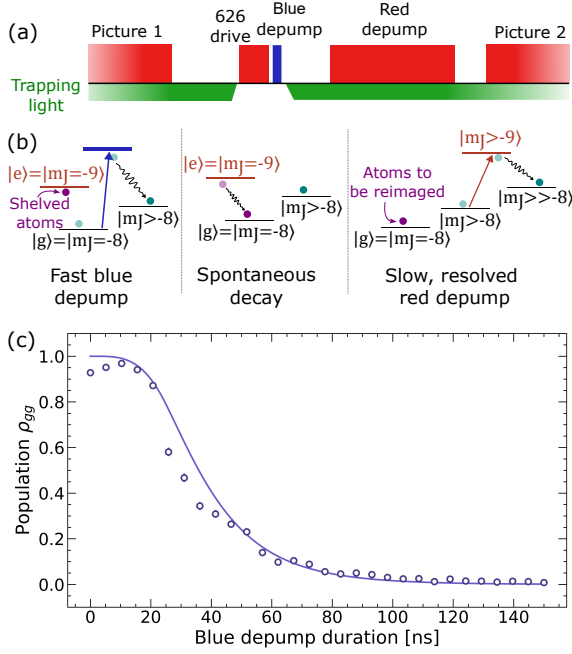


FIG. S2. (a) Pulse sequence for state readout. The experiment is done in time of flight in order to eliminate any systematic errors we may have due to the traps. (b) Internal state dynamics during state readout: atoms in $|g\rangle$ are depumped by a fast pulse of π -polarized light on the broad 421 nm transition. Following this pulse, atoms that were in $|g\rangle$, end up in higher Zeeman states ($m_J > -8$) while atoms that were in $|e\rangle$ have decayed to $|g\rangle$. We apply a second pulse of 626 nm π -polarized light that selectively further depumps atoms in $m_J = -7$ to prevent unintentional further repumping during imaging of the $|g\rangle$ atoms. (c) Calibration of the depumping time. We apply a 421 nm pulse of varying duration, atoms are all in $|g\rangle$ initially, we show the ratio of atoms which survive this pulse. We also plot the solutions to the optical Bloch equations for the $J = 8 \rightarrow J = 9$ transition (36 states) for the evolution of the population of an atom starting in the $|g\rangle = m_J = -8$ state and subject to a pulse of 421 nm light, taking into account the rise time of the EOM we use to turn the blue light on.

in $|g\rangle$ are depumped by the light pulse to other Zeeman states $|d\rangle = |J = 8; m_J > -8\rangle$ (see figure S2 (b)), these atoms are then not re-imaged in subsequent images. The $|e\rangle$ atoms are shelved from the blue pulse, and then decay down to $|g\rangle$, so that they are re-imaged in the second picture. We have observed that atoms that are depumped to $m_J = -7$ but not further might actually be repumped by the imaging light and appear as $|e\rangle$ atoms. To prevent this, we add an extra depumping stage once all the atoms are in the ground state manifold (Fig. S2 (b)). It is performed with π -polarized light on the 626 nm transition. This transition is sufficiently narrow to be selective and depumps atoms in $m_J = -7$ to higher Zeeman states without impacting atoms in $m_J = -8$ (that were originally in $|e\rangle$).

The fidelity of this state readout is limited by the

lifetime of $|e\rangle$. During the 100 ns pulse, a fraction of $|e\rangle$ atoms decay to $|g\rangle$, limiting the fidelity of the state readout. In addition, some $|g\rangle$ atoms might remain in $|g\rangle$. This leads to a probability of measuring an atom in a given state:

$$P(m_x) = P(m_x|x)P(x) + P(m_x|y)P(y) \quad (\text{S1})$$

Where $P(m_x)$ is the probability to measure the atom in state $|x\rangle$ ($x, y = e, g$), $P(m_x|y) = 1 - P(m_y|y)$ is the probability of measuring the atom in $|x\rangle$ while it was actually in $|y\rangle$ and $P(x)$ is the probability for the atom to be in $|x\rangle$. On the experiment, we calibrated $P(m_e|g)$ and $P(m_g|e)$ in the following manner: First, we start with all atoms in $|g\rangle$, we then apply the blue pulse. The fraction of atoms that were not depumped and that we re-image after this gives us $P(m_e) = P(m_e|g) = 0.05$. We show in Fig. S2 how $P(m_e)$ evolves with the time of the blue pulse. In blue solid line, we show the theoretical expectation. This is obtained by calculating the population in $|g\rangle = |J = 8, m_J = -8\rangle$ by solving the master equation of the $J = 8 \rightarrow J' = 9$ system driven by blue light with π polarization and taking into account the rise time of the Pockels cell EOM. The best fit (solid blue line) is obtained by taking a Rabi frequency of $\Omega_{421} = 50$ MHz for the 421 nm light.

Second, we prepare an incoherent mixture of $|g\rangle$ $|e\rangle$ ($P(e) = P(g) = 0.5$) by sending a resonant pulse of 626 nm light with a high Rabi frequency $\Omega = 2\pi \times 3$ MHz for a time $t \gg 1/\Gamma$. We measure $P(m_e)$ and then determine the fidelity, we get $P(m_e|e) = 0.92$. This is in good agreement with our expectations since the fraction of population initially in $|e\rangle$ that decays during the blue pulse and might be depumped is expected to be $e^{-\tau_p/\tau} = 0.92$. We show observed Rabi oscillations in the main text (Fig. 1(c)) when driving the $|g\rangle \rightarrow |e\rangle$ transition with the raw data in blue dots and the data corrected for detection errors using the above calibration in red diamonds. The data are very well fitted by a solution of the optical Bloch equations [46], with Rabi frequency $\Omega = 3.6$ MHz and a transverse decay rate $\gamma_{\perp} = 60$ kHz (with $\Gamma = (2\pi) 135$ kHz). We assign this transverse decay rate to laser phase noise and inhomogeneity of the Rabi frequency among the different atoms.

APPENDIX C: SINGLE-ATOM EXCITATION PROBABILITY ANALYSIS

The data plotted in Fig. 3 is an average of many experimental realizations, sometimes separated by a few weeks. We therefore have to eliminate systematic effects. First, residual inhomogeneities of the site resolved excitation imaging along the chain. For this we calibrate $P^{(i)}(m_e|e)$ and $P^{(i)}(m_g|g)$ at each site (i). We also measure the effect of switching the tweezers off during the red driving light and the blue depump

pulse. We measure $P_S^{(i)}$ the probability for atom i to survive the switch on and off of the tweezers in absence of the drive and depump beams. These quantities are calibrated by interleaved measurements during the data taking. What is finally plotted in Fig. 3 is $P^{(i)}(e)/P_S^{(i)}$. This allows us to eliminate any systematic effects which could be non homogeneous along the atomic chain. Furthermore, the driving laser Rabi frequency was not constant over all datasets. We accounted for it by normalizing the data by the measured probability of the first atom to be excited. We note that since this individual point is prone to statistical noise, this results in a statistical offset of all points, but we use this to keep the data analysis free of adjustable parameters.

APPENDIX D: MEAN-FIELD SIMULATIONS

We perform simulations of the light scattering experiments based on the mean-field equations that can be derived from the full master equation. They are derived in many works, see for instance [10, 47] for more details.

They read:

$$\begin{cases} \frac{d\rho_{ee,n}}{dt} = -\Gamma_0\rho_{ee,n} + \frac{i}{2}(\Omega_n\rho_{eg,n}^* - \Omega_n^*\rho_{eg,n}) \\ \frac{d\rho_{eg,n}}{dt} = -\left(\frac{\Gamma_0}{2} - i\Delta_L\right)\rho_{eg,n} + \frac{i}{2}\Omega_n(1 - 2\rho_{ee,n}) \end{cases} \quad (\text{S1})$$

Ω_n is the total Rabi frequency for atom n . It has two

contributions: the drive, and that of the other dipoles in the chain (called Ω_{atoms} in the main text). It is written in terms of the fields:

$$\Omega_n = \frac{d_0}{\hbar}\vec{\varepsilon}\cdot\vec{E}_{tot} = \frac{d_0}{\hbar}\vec{\varepsilon}\cdot\left(\vec{E}_L + \sum_{k\neq n}\vec{E}_k(\vec{r}_n)\right) \quad (\text{S2})$$

with $\vec{\varepsilon} = (\hat{y} - i\hat{z})/\sqrt{2}$ the polarization of the transition we consider here: σ^- -transition with magnetic field along \hat{x} . \vec{E}_L is the laser field and $\vec{E}_k(\vec{r}_n)$ is the field radiated by atom k on atom n . The dipole-dipole interaction between two atoms used in the main text is given by $V_{dd}(\vec{r}_n - \vec{r}_m) = -\vec{d}_n\cdot\vec{E}_m(\vec{r}_n - \vec{r}_m)$ [10]. The field of atom k is $\vec{E}_k(\vec{r}_n) = \overleftrightarrow{\mathbf{G}}(\mathbf{r}_n - \mathbf{r}_k)\cdot\vec{\varepsilon}^*$ with the Green's function:

$$\begin{aligned} \overleftrightarrow{\mathbf{G}}(\mathbf{r}) &= \frac{k^3}{4\pi\epsilon_0}e^{ikr}\left(\frac{1}{kr} + \frac{i}{(kr)^2} - \frac{1}{(kr)^3}\right)\mathbb{I} \\ &+ \frac{k^3}{4\pi\epsilon_0}e^{ikr}\left(-\frac{1}{kr} - \frac{3i}{(kr)^2} + \frac{3}{(kr)^3}\right)|\hat{\mathbf{r}}\rangle\langle\hat{\mathbf{r}}|. \end{aligned}$$

The 30 atoms of the chain have positions $\vec{r}_i = \vec{r}_{0,i} + \vec{\delta}r_i$, where $(\vec{r}_{0,i})_{i\in[0,N-1]}$ are the positions of the 30 tweezers perfectly spaced by d . To average on positional disorder due to temperature, we draw the random positions $\vec{\delta}r_i$ following the Boltzmann distribution $\exp\left(-\frac{m\omega^2 r^2}{2k_B T}\right)$. We have further verified in the linear regime that accounting for Doppler broadening due to thermal motion does not lead to a significant reduction of the calculated shifts.

-
- [1] R. H. Dicke, Coherence in spontaneous radiation processes, *Phys. Rev.* **93**, 99 (1954).
 - [2] Superradiance: An essay on the theory of collective spontaneous emission, *Physics Reports* **93**, 301 (1982).
 - [3] L. Allen and J. H. Eberly, *Optical resonance and two-level atoms* (Dover, 1987).
 - [4] R. Friedberg, S. Hartmann, and J. Manassah, Frequency shifts in emission and absorption by resonant systems of two-level atoms, *Physics Reports* **7**, 101 (1973).
 - [5] Z. Meir, O. Schwartz, E. Shahmoon, D. Oron, and R. Ozeri, Cooperative lamb shift in a mesoscopic atomic array, *Phys. Rev. Lett.* **113**, 193002 (2014).
 - [6] S. L. Bromley, B. Zhu, M. Bishof, X. Zhang, T. Bothwell, J. Schachenmayer, T. L. Nicholson, R. Kaiser, S. F. Yelin, M. D. Lukin, A. M. Rey, and J. Ye, Collective atomic scattering and motional effects in a dense coherent medium, *Nature Communications* **7**, 11039 (2016).
 - [7] S. Jennewein, M. Besbes, N. J. Schilder, S. D. Jenkins, C. Sauvan, J. Ruostekoski, J.-J. Greffet, Y. R. P. Sortais, and A. Browaeys, Coherent scattering of near-resonant light by a dense microscopic cold atomic cloud, *Phys. Rev. Lett.* **116**, 233601 (2016).
 - [8] L. Corman, J. L. Ville, R. Saint-Jalm, M. Aidelsburger, T. Bienaimé, S. Nascimbène, J. Dalibard, and J. Beugnon, Transmission of near-resonant light through a dense slab of cold atoms, *Phys. Rev. A* **96**, 053629 (2017).
 - [9] T. Peyrot, Y. R. P. Sortais, A. Browaeys, A. Sargsyan, D. Sarkisyan, J. Keaveney, I. G. Hughes, and C. S. Adams, Collective lamb shift of a nanoscale atomic vapor layer within a sapphire cavity, *Phys. Rev. Lett.* **120**, 243401 (2018).
 - [10] A. Glicenstein, G. Ferioli, N. Šibalić, L. Brossard, I. Ferrier-Barbut, and A. Browaeys, Collective shift in resonant light scattering by a one-dimensional atomic chain, *Phys. Rev. Lett.* **124**, 253602 (2020).
 - [11] A. Skljarrow, H. Kübler, C. S. Adams, T. Pfau, R. Löw, and H. Alaeian, Purcell-enhanced dipolar interactions in nanostructures, *Phys. Rev. Res.* **4**, 023073 (2022).
 - [12] R. Vatré, R. Lopes, J. Beugnon, and F. Gerbier, *Resonant light scattering by a slab of ultracold atoms* (2024), arXiv:2409.04148 [cond-mat.quant-gas].
 - [13] D. E. Chang, J. Ye, and M. D. Lukin, Controlling dipole-dipole frequency shifts in a lattice-based optical atomic clock, *Phys. Rev. A* **69**, 023810 (2004).
 - [14] S. Krämer, L. Ostermann, and H. Ritsch, Optimized geometries for future generation optical lattice clocks, *Europhysics Letters* **114**, 14003 (2016).
 - [15] A. Cidrim, A. Piñeiro Orioli, C. Sanner, R. B. Hut-

- son, J. Ye, R. Bachelard, and A. M. Rey, Dipole-dipole frequency shifts in multilevel atoms, *Phys. Rev. Lett.* **127**, 013401 (2021).
- [16] R. B. Hutson, W. R. Milner, L. Yan, J. Ye, and C. Sanner, Observation of millihertz-level cooperative lamb shifts in an optical atomic clock, *Science* **383**, 384 (2024).
- [17] G. Facchinetti and J. Ruostekoski, Interaction of light with planar lattices of atoms: Reflection, transmission, and cooperative magnetometry, *Phys. Rev. A* **97**, 023833 (2018).
- [18] R. J. Bettles, S. A. Gardiner, and C. S. Adams, Cooperative eigenmodes and scattering in one-dimensional atomic arrays, *Phys. Rev. A* **94**, 043844 (2016).
- [19] R. J. Bettles, S. A. Gardiner, and C. S. Adams, Enhanced optical cross section via collective coupling of atomic dipoles in a 2d array, *Phys. Rev. Lett.* **116**, 103602 (2016).
- [20] E. Shahmoon, D. S. Wild, M. D. Lukin, and S. F. Yelin, Cooperative resonances in light scattering from two-dimensional atomic arrays, *Phys. Rev. Lett.* **118**, 113601 (2017).
- [21] A. Asenjo-Garcia, M. Moreno-Cardoner, A. Albrecht, H. J. Kimble, and D. E. Chang, Exponential improvement in photon storage fidelities using subradiance and “selective radiance” in atomic arrays, *Phys. Rev. X* **7**, 031024 (2017).
- [22] J. Rui, D. Wei, A. Rubio-Abadal, S. Hollerith, J. Zeiher, D. M. Stamper-Kurn, C. Gross, and I. Bloch, A subradiant optical mirror formed by a single structured atomic layer, *Nature* **583**, 369 (2020).
- [23] K. Srakaew, P. Weckesser, S. Hollerith, D. Wei, D. Adler, I. Bloch, and J. Zeiher, A subwavelength atomic array switched by a single rydberg atom, *Nature Physics* **19**, 714 (2023).
- [24] A. Glicenstein, A. Apoorva, D. B. Orenes, H. Letellier, A. M. G. de Melo, R. Saint-Jalm, and R. Kaiser, *In-situ measurements of light diffusion in an optically dense atomic ensemble* (2024), arXiv:2409.11117 [physics.atom-ph].
- [25] D. Bloch, B. Hofer, S. R. Cohen, A. Browaeys, and I. Ferrier-Barbut, Trapping and imaging single dysprosium atoms in optical tweezer arrays, *Phys. Rev. Lett.* **131**, 203401 (2023).
- [26] D. Bloch, B. Hofer, S. R. Cohen, M. Lepers, A. Browaeys, and I. Ferrier-Barbut, Anisotropic polarizability of dy at 532 nm on the intercombination transition, *Phys. Rev. A* **110**, 033103 (2024).
- [27] M. Endres, H. Bernien, A. Keesling, H. Levine, E. R. Anschuetz, A. Krajenbrink, C. Senko, V. Vuletic, M. Greiner, and M. D. Lukin, Atom-by-atom assembly of defect-free one-dimensional cold atom arrays, *Science* **354**, 1024 (2016).
- [28] A. W. Young, W. J. Eckner, N. Schine, A. M. Childs, and A. M. Kaufman, Tweezer-programmable 2d quantum walks in a hubbard-regime lattice, *Science* **377**, 885 (2022).
- [29] A. Kramida, Yu. Ralchenko, J. Reader, and and NIST ASD Team, NIST Atomic Spectra Database (ver. 5.12), [Online]. Available: <https://physics.nist.gov/asd> [2024, November 13]. National Institute of Standards and Technology, Gaithersburg, MD. (2024).
- [30] M. Kiffner, M. Macovei, J. Evers, and C. Keitel, Chapter 3 - vacuum-induced processes in multilevel atoms (Elsevier, 2010) pp. 85–197.
- [31] W. Nagourney, J. Sandberg, and H. Dehmelt, Shelved optical electron amplifier: Observation of quantum jumps, *Phys. Rev. Lett.* **56**, 2797 (1986).
- [32] T. Sauter, W. Neuhauser, R. Blatt, and P. E. Toschek, Observation of quantum jumps, *Phys. Rev. Lett.* **57**, 1696 (1986).
- [33] R. T. Sutherland and F. Robicheaux, Collective dipole-dipole interactions in an atomic array, *Physical Review A* **94**, 10.1103/physreva.94.013847 (2016).
- [34] J. Ruostekoski and J. Javanainen, Quantum field theory of cooperative atom response: Low light intensity, *Phys. Rev. A* **55**, 513 (1997).
- [35] Y.-X. Zhang and K. Mølmer, Theory of subradiant states of a one-dimensional two-level atom chain, *Phys. Rev. Lett.* **122**, 203605 (2019).
- [36] L. Henriët, J. S. Douglas, D. E. Chang, and A. Albrecht, Critical open-system dynamics in a one-dimensional optical-lattice clock, *Phys. Rev. A* **99**, 023802 (2019).
- [37] A. S. Sheremet, M. I. Petrov, I. V. Iorsh, A. V. Poshakinskiy, and A. N. Poddubny, Waveguide quantum electrodynamics: Collective radiance and photon-photon correlations, *Rev. Mod. Phys.* **95**, 015002 (2023).
- [38] We fit the simulation results in the same 500 kHz window as in the experiment. For a large Rabi frequency we find that the shift obtained in the simulation results depends on the fit window, indicating that the line is not Lorentzian. In the future it would be interesting to explore the line distortion experimentally.
- [39] We observed systematic shifts which we ascribe to a slow turn-off of the lattice, which plays a much stronger role in Ramsey interferometry with respect to the slow steady-state experiments above.
- [40] This model assumes that the decay rate is not modified by collective effects.
- [41] S. J. Masson, I. Ferrier-Barbut, L. A. Orozco, A. Browaeys, and A. Asenjo-Garcia, Many-body signatures of collective decay in atomic chains, *Phys. Rev. Lett.* **125**, 263601 (2020).
- [42] B. Olmos, D. Yu, and I. Lesanovsky, Steady-state properties of a driven atomic ensemble with nonlocal dissipation, *Phys. Rev. A* **89**, 023616 (2014).
- [43] C. D. Parmee and N. R. Cooper, Phases of driven two-level systems with nonlocal dissipation, *Phys. Rev. A* **97**, 053616 (2018).
- [44] C. D. Parmee and J. Ruostekoski, Signatures of optical phase transitions in superradiant and subradiant atomic arrays, *Communications Physics* **3**, 205 (2020).
- [45] V. Zhang, S. Ostermann, O. Rubies-Bigorda, and S. F. Yelin, *Emergent limit cycles, chaos, and bistability in driven-dissipative atomic arrays* (2024), arXiv:2406.19168 [quant-ph].
- [46] D. Steck, *Quantum and Atom Optics* (2007).
- [47] T. S. do Espirito Santo, P. Weiss, A. Cipris, R. Kaiser, W. Guerin, R. Bachelard, and J. Schachenmayer, Collective excitation dynamics of a cold atom cloud, *Phys. Rev. A* **101**, 013617 (2020).